Antiresorptive activity of osteoprotegerin requires an intact heparan sulfate-binding site

Miaomiao Li[a] and Ding Xu[a,1]

[a]Department of Oral Biology, School of Dental Medicine, University at Buffalo, The State University of New York, Buffalo, NY 14214

Edited by Zena Werb, University of California San Francisco Medical Center, San Francisco, CA, and approved June 11, 2020 (received for review March 28, 2020)

Osteoprotegerin (OPG), a secreted decoy receptor for receptor activator of nuclear factor B ligand (RANKL), plays an essential role in regulating bone resorption. While much is known about the function of the N-terminal domains of OPG, which is responsible for binding to RANKL, the exact biological functions of the three C-terminal domains of OPG remain uncertain. We have previously shown that one likely function of the C-terminal domains of OPG is to bind cell surface heparan sulfate (HS), but the in vivo evidence was lacking. To investigate the biological significance of OPG–HS interaction in bone remodeling, we created OPG knock-in mice (opg^{AAA}). The mutated OPG is incapable of binding to HS but binds RANKL normally. Surprisingly, $opg^{AAA/AAA}$ mice displayed a severe osteoporotic phenotype that is very similar to *opg*-null mice, suggesting that the antiresorption activity of OPG requires HS. Mechanistically, we propose that the HS immobilizes secreted OPG at the surface of osteoblasts lineage cells, which facilitates binding of OPG to membrane-anchored RANKL. To further support this model, we altered the structure of osteoblast HS genetically to make it incapable of binding to OPG. Interestingly, *osteocalcin-Cre;Hs2st*$^{f/f}$ mice also displayed osteoporotic phenotype with similar severity to $opg^{AAA/AAA}$ mice. Combined, our data provide strong genetic evidence that OPG–HS interaction is indispensable for normal bone homeostasis.

heparan sulfate | OPG | RANKL | H2st | osteoclast

Osteoprotegerin (OPG) is one of the most important regulators of bone remodeling. As a decoy receptor, it functions by neutralizing the activity of receptor activator of nuclear factor B ligand (RANKL). To drive osteoclastogenesis, RANKL needs to bind and activate receptor activator of nuclear factor B (RANK) expressed by osteoclast precursors. When OPG is present, it limits the bioavailability of RANKL and effectively inhibits osteoclastogenesis (1, 2). The role of OPG as a master negative regulator of osteoclastogenesis is manifested by the profound osteoporosis phenotype displayed by $opg^{-/-}$ mice, which stems from the uncontrolled osteoclastogenesis and bone resorption (3, 4).

Like other tumor necrosis factor (TNF) family members, RANKL is expressed as a transmembrane cytokine (2, 5). Although a soluble form of RANKL does exist in vivo, and it has been used routinely in vitro to drive osteoclastogenesis, a recent study has shown definitively that the transmembrane form of RANKL expressed by osteoblast lineage cells is required for osteoclastogenesis in vivo (6). In contrast, although a member of the TNF receptor family, OPG is notably the only member that is expressed as a secreted soluble factor. Our previous in vitro work has shown that for OPG to efficiently inhibit RANKL at physiologically relevant concentration, OPG needs to bind heparan sulfate proteoglycan (HSPG) expressed by osteoblast lineage cells (7). We propose that binding to osteoblast cell surface heparan sulfate (HS) provides a means for OPG to be immobilized onto the cell membrane, which keeps it in close proximity to membrane-attached RANKL and facilitates efficient inhibition of RANKL.

HS is a linear sulfated polysaccharide expressed by all mammalian cells and it exists as glycoconjugates by covalently linked to a large number of core proteins (8, 9). HS can be found abundantly on the cell membrane and in the extracellular matrix and it performs biological functions by interacting with hundreds of HS-binding proteins (10). Binding to HS often provides another dimension of regulation on the structure and function of HS-binding proteins. Many proteins that play essential roles in bone development are well-known HS-binding proteins, which includes hedgehog, BMP, Wnt, and FGF2. Indeed, almost all transgenic mice with altered HS structures showed defects in skeleton development, which demonstrates the critical role of HS in regulating bone development (11–14). Because global knockout of essential HS biosynthetic enzymes leads to prenatal or neonatal lethality, the exact role of HS in bone remodeling remains largely unknown due to lack of appropriate animal models.

Here, by using an OPG knock-in mice (opg^{AAA}) and an osteoblast lineage conditional knockout of heparan sulfate 2-*O*-sulfotransferease (Hs2st), we report that one essential role of HS in bone remodeling is to facilitate the antiresorptive function of OPG. The opg^{AAA} knock-in mice express an OPG variant that displays impaired binding to HS but normal binding to RANKL. Our analysis showed that the opg^{AAA} knock-in mice display an osteoporotic phenotype that is similar to the $opg^{-/-}$ mice, which strongly suggests that OPG–HS interaction is required for the biological function of OPG in bone remodeling. This conclusion is further supported by the bone phenotype of *osteocalcin-Cre (Oc-Cre);Hs2st*$^{f/f}$ mice, which phenocopies the osteoporotic phenotype of opg^{AAA} knock-in mice. The osteoporotic phenotype of

Significance

Osteoprotegerin (OPG) plays an essential role in bone remodeling by inhibiting receptor activator of nuclear factor B ligand (RANKL), which drives osteoclastogenesis. While much is known about OPG–RANKL interaction, the exact biological function of the C-terminal domains of OPG remains a mystery. One likely function of the C-terminal domains of OPG is to interact with heparan sulfate (HS), a glycosaminoglycan that is abundantly expressed by osteoblast lineage cells. However, the physiological importance of OPG–HS interactions in bone remodeling remains uncertain. Here, by using two strains of transgenic mice, both of which have altered OPG–HS interactions, we have definitively shown that binding to osteoblast HS is indispensable for the antiresorptive function of OPG in bone remodeling.

Author contributions: M.L. and D.X. designed research; M.L. performed research; M.L. and D.X. analyzed data; and M.L. and D.X. wrote the paper.

The authors declare no competing interest.

This article is a PNAS Direct Submission.

[1]To whom correspondence may be addressed. Email: dingxu@buffalo.edu.

This article contains supporting information online at https://www.pnas.org/lookup/suppl/doi:10.1073/pnas.2005859117/-/DCSupplemental.

First published July 7, 2020.

Oc-Cre;Hs2st$^{f/f}$ mice also confirms that HS expressed by osteoblast lineage cells is required for the biological function of OPG.

Results

Characterization of an HS Binding-Deficient OPG. OPG is a multi-domain protein with four N-terminal cysteine-rich domains (CRDs), followed by two death-like domains (D1 and D2) and a short C-terminal tail domain (Fig. 1*A*). We and others have previously determined that the CRDs are responsible for RANKL binding, while the D2 and tail domain are responsible for binding to HS (7, 15–18). Eight basic amino acid residues have been identified to mediate HS binding in OPG (Fig. 1*A*). Here, we prepared a triple mutant of murine OPG (mOPG) bearing R366A, K367A, and R370A mutations (OPG^{AAA}). As expected, OPG^{AAA} almost completely loses the capacity to bind cell surface HS (Fig. 1*B*) while maintaining wild type (WT)-like binding affinity to RANKL (apparent binding affinity 0.15 vs. 0.21 nM) (Fig. 1*C*).

***opg*$^{AAA/AAA}$ Mice Show Severe Osteoporosis.** To generate a murine model to specifically dissect the contribution of HS–OPG interaction in bone remodeling, we have introduced R366A–K367A–R370A triple mutations into the *opg* locus by clustered regularly interspaced short palindromic repeats (CRISPR)–mediated homologous recombination (Fig. 1*D*). *opg*$^{AAA/AAA}$ mice were born with normal litter size and grew normally without gross morphological abnormalities. The serum concentration of OPG in *opg*$^{AAA/AAA}$ mice was very similar to the OPG concentration in WT mice (Fig. 1*E*), which suggests that the mutation did not negatively affect the expression and secretion of OPG.

Radiographic examination of the 10-wk-old male mice indicated that the *opg*$^{AAA/AAA}$ mice had substantially reduced trabecular bone

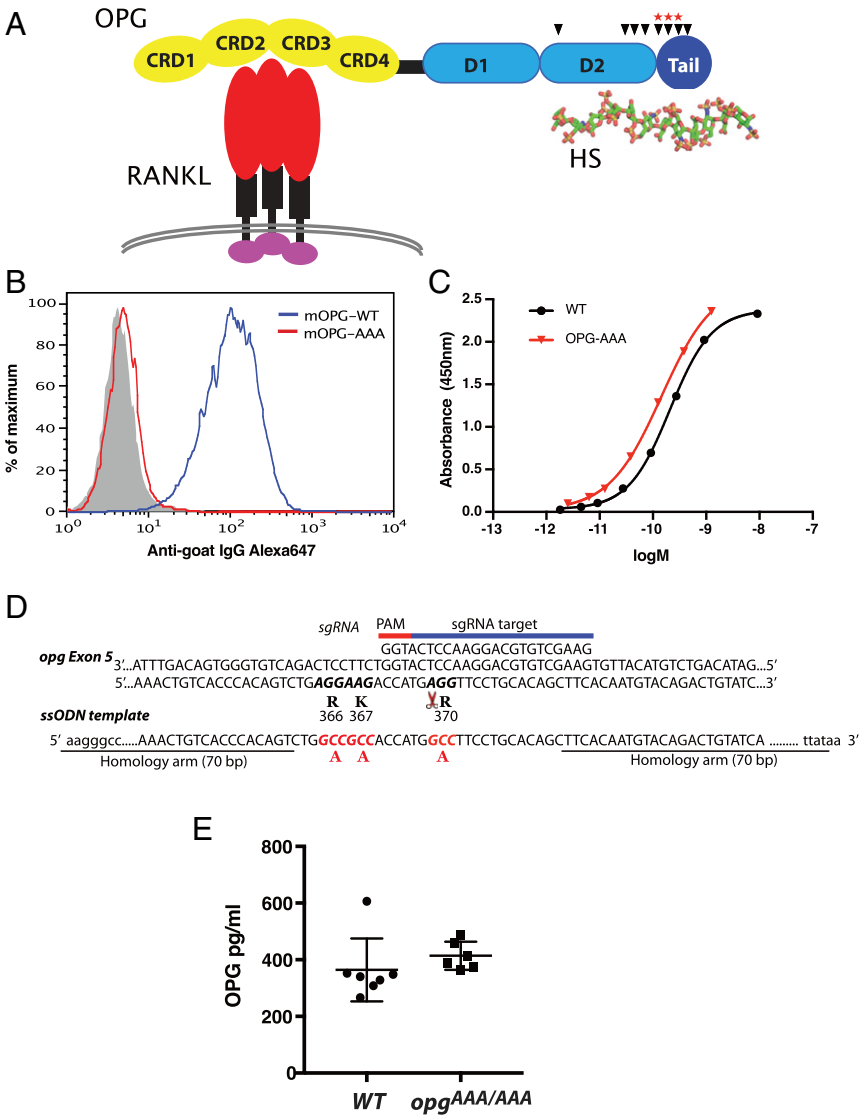

Fig. 1. Characterization of HS binding-deficient OPG mutant and generation of *opg*^{AAA} knock-in mice. (*A*) Schematic view of the domain structure of OPG. Binding to RANKL is mediated by the N-terminal CRD domains, while HS binding is mediated by D2 and C-terminal tail domains. The relative positions of the HS-binding residues are marked with arrowheads. Locations of R366, K367, and R370 are marked by red stars. (*B*) Binding of recombinant WT mouse OPG (mOPG-WT) or mOPG-AAA triple mutant (20 ng/mL) to MC3T3 cells was determined by a fluorescence-activated cell sorting (FACS)-based binding assay. IgG, immuoglobulin G. (*C*) Binding affinity of mOPG-WT and mOPG-AAA to immobilized RANKL was determined by enzyme-linked immunosorbent assay (ELISA). (*D*) Targeting strategy for generating *opg*^{AAA} knock-in mice. Sequences of the targeting single guide RNA (sgRNA), the mutation sites in *opg* exon 5, and the repairing template single-stranded donor oligonucleotides (ssODN) are shown. (*E*) Serum concentrations of OPG were quantified by sandwich ELISA. All values are from 10-wk-old male mice.

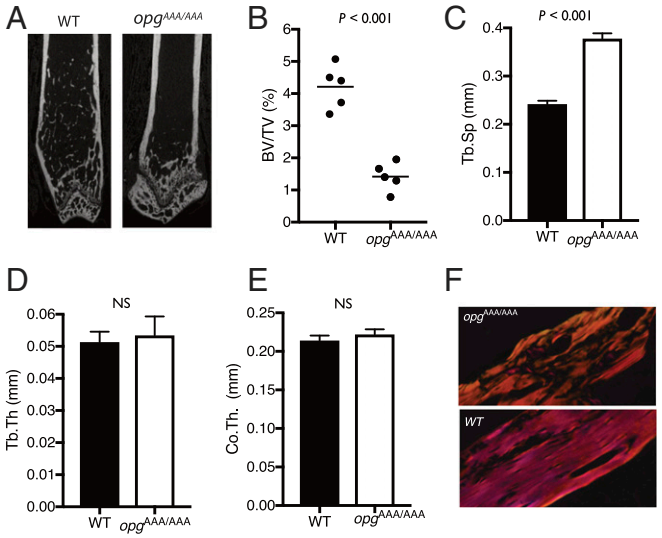

Fig. 2. $opg^{AAA/AAA}$ mice develop osteoporosis. (*A*) Representative μCT images of the femurs. (*B*) Trabecular BV/TV of femurs. (*C*) Trabecular separation (Tb.Sp), (*D*) trabecular thickness (Tb.Th), and (*E*) cortical thickness (Co.Th.) of femurs. All values are from 10-wk-old male mice. $n = 5$. Error bars represent SD. *P* value was determined by two-way Student's *t* test. NS, not significant. (*F*) Polarized light microscopy of cortical bone shows woven pattern in opg^{AAA} mice and lamellar pattern in WT mice.

in both femur and vertebra (*SI Appendix*, Fig. S1 *A* and *B*). Microcomputed tomography (μCT) analysis of femur confirmed that compared with WT mice, $opg^{AAA/AAA}$ mice displayed a threefold reduction in bone volume over tissue volume (BV/TV) value (1.4 vs. 4.2%) (Fig. 2 *A* and *B*). Similar osteoporotic phenotype was observed in 10-wk-old female mice (*SI Appendix*, Fig. S2). We next examined the microstructure of the trabecular bone and found that the separation of trabecular bone was increased by 58% compared with WT mice (Fig. 2*C*). In contrast, the trabecular thickness was not altered in $opg^{AAA/AAA}$ mice (Fig. 2*D*). While we did not observe a difference in cortical bone thickness between $opg^{AAA/AAA}$ mice and WT mice (Fig. 2*E*), we found that the collagen fiber organization was altered in $opg^{AAA/AAA}$ mice. Under polarized light microscopy, the birefringence was sparse in the cortical bone of $opg^{AAA/AAA}$ mice, indicating shorter/less organized collagen fibers often associated with woven bone. In contrast, the cortical bone of WT mice had well-organized collagen fibers typical of lamellar bone (Fig. 2*F*). We further confirmed that the osteoporotic phenotype of $opg^{AAA/AAA}$ mice was already apparent when mice were as young as 4 wk old (*SI Appendix*, Fig. S1*D*). Interestingly, different from the 10-wk-old mice, we observed a slight decrease of cortical bone thickness and femur length in 4-wk-old $opg^{AAA/AAA}$ mice (*SI Appendix*, Fig. S1 *E* and *F*). Our result strongly suggests that interaction with HS is required for OPG to perform its normal antiresorptive function. At last, we also checked the mineral apposition rate of $opg^{AAA/AAA}$ mice and found that it was comparable with the WT mice (*SI Appendix*, Fig. S3*A*).

Osteoclastogenesis Is Enhanced in $opg^{AAA/AAA}$ Mice. Tartrate-resistant acid phosphatase (TRAP) staining of tibia sections showed that the number of osteoclasts in $opg^{AAA/AAA}$ mice was increased by 60% (Fig. 3 *A*–*C*), which indicates that enhanced bone resorption is the main driver of the osteoporotic phenotype. As shown in Fig. 3*B*, many trabeculae in $opg^{AAA/AAA}$ tibia were swamped by osteoclasts, which were rarely observed in WT tibia (Fig. 3*A*). As OPG is mainly expressed by osteoblast cells, we performed an osteoblast/bone marrow macrophage (BMM) coculture assay to examine whether OPG^{AAA} is truly ineffective in inhibiting osteoclastogenesis. In this model, primary calvarial osteoblasts from WT and $opg^{AAA/AAA}$ were cultured with WT BMM. Compared with WT osteoblasts, BMM cultured with $opg^{AAA/AAA}$ osteoblasts formed much bigger TRAP-positive cells with more nucleus (Fig. 3 *D* and *E*), and they displayed 33% increase in TRAP activity (Fig. 3*F*). This result strongly suggests that compared with WT OPG, OPG^{AAA} is less effective in inhibiting RANKL displayed on osteoblast surface, which resulted in exaggerated osteoclastogenesis.

Osteoblast HS Promotes OPG–RANKL Complex Formation. The osteoporotic phenotype of $opg^{AAA/AAA}$ mice supports a model where osteoblast HSPGs helps localize secreted OPG to cell surface and promote OPG–RANKL interaction (Fig. 4*A*). This model would predict that the osteoblast HS is located in close proximity to cell surface RANKL in order to promote OPG–RANKL interaction. Indeed, using MC3T3 cells stably expressing RANKL, we found that RANKL and HS show extensive colocalization (Fig. 4*B*). To quantitatively determine whether HS promotes OPG–RANKL interaction on osteoblast cell surface, we performed a Duolink proximity ligation assay (PLA). In this assay, each OPG–RANKL interaction (or very close association) will give rise to an intense fluorescence dot, which can be quantified to assess the extent of OPG–RANKL interactions. When MC3T3 cells were pretreated with heparin lyase III (HL-III), which removes cell surface HS, the PLA signal was reduced by 43% (Fig. 4*C*). Similarly, when MC3T3 cells were preincubated with mOPG-AAA mutant instead of mOPG-WT, the PLA signals were also reduced by 53% (Fig. 4*D*). These results directly support our model and strongly suggest that HS promotes OPG–RANKL interaction at osteoblast cell surface. We further determined that murine osteoblasts mainly express two types of HSPGs, syndecan-1 and syndecan-4 (*SI Appendix*, Fig. S4), which suggests that both syndecans could be involved in promoting OPG–RANKL interactions.

2-*O*-Sulfation Is Required for OPG Binding to Osteoblast HS. The main structural element that mediates HS–protein interactions is the sulfate group. Sulfation can occur at *N*, 6-*O*, and 3-*O* positions of *N*-acetyl glucosamine and at the 2-*O* position of iduronic acid (8). For some HS-binding proteins, their binding to HS requires sulfation at very specific positions. For example, binding of basic fibroblast growth factor (bFGF) to HS requires 2-*O*-sulfation of iduronic acid (19). We have previously determined that the sulfate group at 2-*O*-sulfation also plays a critical role in mediating HS–OPG interactions by using 2-*O*-sulfation–deficient CHO cells (7). To verify that this is also true in osteoblast lineage cells, we generated a 2-*O*-sulfation–deficient MC3T3 cell line using the CRISPR-Cas9 system by introducing in-del mutations to *Hs2st*. $MC3T3^{\Delta hs2st}$ cells displayed a 94% reduction in bFGF binding compared with MC3T3-WT cells (relative fluorescence units = 40 vs. 690) (Fig. 5*A*), which confirms that $MC3T3^{\Delta hs2st}$ cells are deficient in 2-*O*-sulfation. As expected, the binding of mOPG to $MC3T3^{\Delta hs2st}$ was reduced about 91% (relative fluorescence units = 2.6 vs. 30) (Fig. 5*B*), which confirms that OPG binding to osteoblast HS also requires 2-*O*-sulfation. Of note, deficiency of Hs2st in MC3T3 cells had minimal effect on the overall sulfation level and quantity of the HS expressed by MC3T3 cells as suggested by HS-specific monoclonal antibody (mAb) 10E4 (*SI Appendix*, Fig. S5), the binding of which to HS does not depends on 2-*O*-sulfation (20).

***Oc-Cre;Hs2st*$^{f/f}$ Mice Develop Osteoporosis.** To assess the role of osteoblast lineage HS in regulating OPG–RANKL interactions, we have crossed the *Oc-Cre* transgenic line with $Hs2st^{flox/flox}$ mice (21). In $Oc\text{-}Cre;Hs2st^{f/f}$ mice, *Hs2st* is deleted in osteoblast lineage cells, including osteoblasts and osteocytes, and also likely in hypertrophic chondrocytes. $Oc\text{-}Cre;Hs2st^{f/f}$ mice were born with

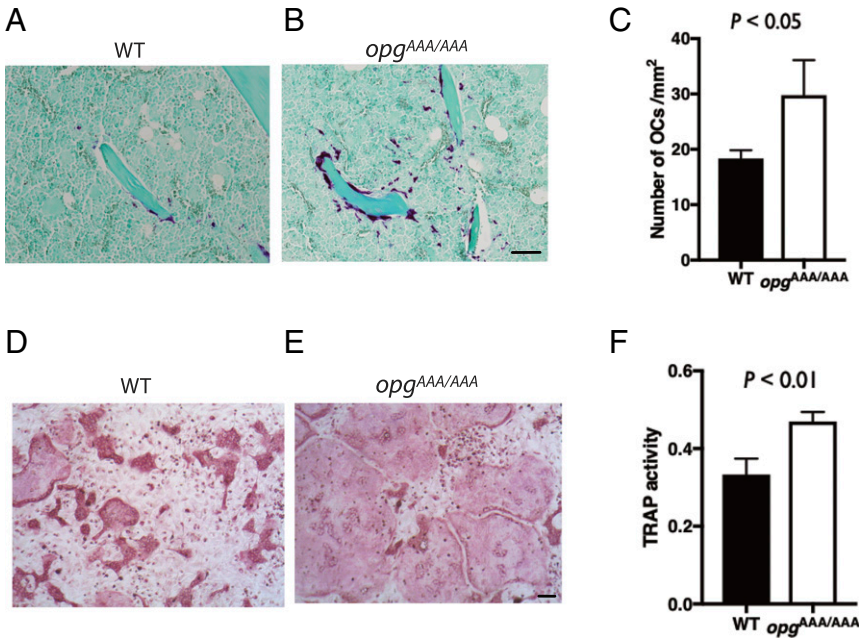

Fig. 3. Osteoclastogenesis is enhanced in $opg^{AAA/AAA}$ mice. (*A* and *B*) TRAP staining of paraffin sections of WT and $opg^{AAA/AAA}$ tibias. Mature osteoclasts were stained purple, and bone was counterstained with Fast Green. (*C*) Quantification of osteoclasts (OCs) in tibia sections. $n = 6$. (*D* and *E*) Osteoblasts isolated from WT or $opg^{AAA/AAA}$ mice cocultured with WT BMMs. Mature osteoclasts are visualized by TRAP staining. (*F*) The extent of osteoclastogenesis in coculture was assessed by an enzymatic assay of TRAP activity in whole-cell lysate. $n = 3$. Error bars represent SD. *P* value was determined by two-way Student's *t* test. Data are representative of at least three separate assays. (Scale bars, 50 μm.)

normal litter size and grew normally without gross morphological abnormalities. Radiographic examination found that like *Oc-Cre;Hs2st*$^{f/f}$, mice had substantially reduced trabecular bone in both vertebra and femur (*SI Appendix*, Fig. S6 *A* and *B*). μCT analysis of 10-wk male mice found that the BV/TV value of *Oc-Cre;Hs2st*$^{f/f}$ mice was reduced approximately threefold compared with littermate control (1.56 vs. 4.5%) (Fig. 5 *C* and *D*), which was highly similar to the extent of reduction in BV/TV value observed in $opg^{AAA/AAA}$ mice (Fig. 2*B*). The trabecular separation of *Oc-Cre;Hs2st*$^{f/f}$ mice was increased by 40% compared with *Hs2st*$^{f/f}$ mice, while the trabecular and cortical thicknesses were not altered in *Oc-Cre;Hs2st*$^{f/f}$ mice (Fig. 5 *E*–*G*). The osteoporotic phenotype of *Oc-Cre;Hs2st*$^{f/f}$ mice was also apparent in 4-wk-old mice, and in these younger mice, the cortical thickness and femur length were also slightly reduced (*SI Appendix*, Fig. S6 *D*–*F*). Similar to $opg^{AAA/AAA}$ mice, we observed that the cortical bone of *Oc-Cre;Hs2st*$^{f/f}$ mice also had shorter/less organized collagen fibers (Fig. 5*H*). In addition, the deletion of *Hs2st* in osteoblast lineage cells did not seem to have an impact on bone formation as examined by fluorochrome double labeling (*SI Appendix*, Fig. S3*B*). The phenotypic similarity between *Oc-Cre*;*Hs2st*$^{f/f}$ and $opg^{AAA/AAA}$ mice strongly suggests that the sulfate group at the 2-*O* position of HS plays critical roles in immobilizing OPG and promoting OPG–RANKL interactions.

Osteoclastogenesis Is Enhanced in Oc-Cre;*Hs2st*$^{f/f}$ Mice. Similar to what was observed in $opg^{AAA/AAA}$ mice, we found that many trabeculae in *Oc-Cre;Hs2st*$^{f/f}$ tibia were swamped by osteoclasts and that the number of osteoclasts in *Oc-Cre;Hs2st*$^{f/f}$ mice was increased by 50% (Fig. 6 *A*–*C*). To further examine whether deficiency in 2-*O*-sulfation in osteoblasts truly impairs the inhibitory activity of OPG, we have prepared *Hs2st*-null and control osteoblasts by infecting osteoblasts with either Cre-expressing or GFP-expressing adenovirus. *Hs2st*-null and *Hs2st*$^{f/f}$ osteoblasts were cocultured with BMM isolated from WT mice. Indeed, the size of TRAP-positive cells was significantly larger in cocultures with *Hs2st*-null osteoblasts compared with cocultures with green fluorescent protein (GFP)-adenovirus–infected osteoblasts (Fig. 6 *D* and *E*), and the TRAP activity was also increased 120% for cocultures with *Hs2st*-null osteoblasts (Fig. 6*F*). Together, our data suggest that 2-*O* sulfation of osteoblast HS plays an antiosteoclastogenic role.

Discussion

OPG was shown to be an HS-binding protein not long after it was identified in the late 1990s (22). However, the biological significance of OPG–HS interaction in bone remodeling remained unclear until recently. By mapping the HS-binding domain of OPG and generating an HS binding-deficient OPG variant, we show in vitro using a coculture system that OPG–HS interaction greatly promotes the inhibitory effect of OPG toward RANKL (7). We hypothesized that HS promotes OPG–RANKL interaction by immobilizing secreted OPG on osteoblast surface, which keeps it in close proximity to the membrane-attached RANKL to allow efficient interactions. To test our hypothesis in vivo, we have created two mice strains to disrupt the OPG–HS interactions and examined the bone remodeling phenotypes of these mice. $opg^{AAA/AAA}$ mice express an HS binding-deficient (but RANKL binding-sufficient) (Fig. 1) variant of OPG, while *Oc-Cre;Hs2st*$^{f/f}$ mice express an OPG binding-deficient form of HS specifically on osteoblast lineage cells. These two strains allowed us to interrogate the biological significance of OPG–HS interactions from both sides of the interaction, which to our knowledge, has not been carried out in any other HS-binding proteins.

The osteoporotic phenotypes we have observed in $opg^{AAA/AAA}$ mice and *Oc-Cre;Hs2st*$^{f/f}$ mice are striking in several regards. First, we found that the severity of the osteoporotic phenotype was highly similar between $opg^{AAA/AAA}$ mice and *Oc-Cre;Hs2st*$^{f/f}$ mice and that the alterations in trabecular and cortical structure also mirrored each other (Figs. 2 and 5). Also, both genotypes exhibited exaggerated osteoclastogenesis to similar extent in vivo and in vitro (Figs. 3 and 6). At last, the osteoporotic phenotype displayed by $opg^{AAA/AAA}$ mice is also highly similar to what was reported for $opg^{-/-}$ mice, whose osteoporotic phenotype also started at around 4 wk of age and resulted in a similar extent of

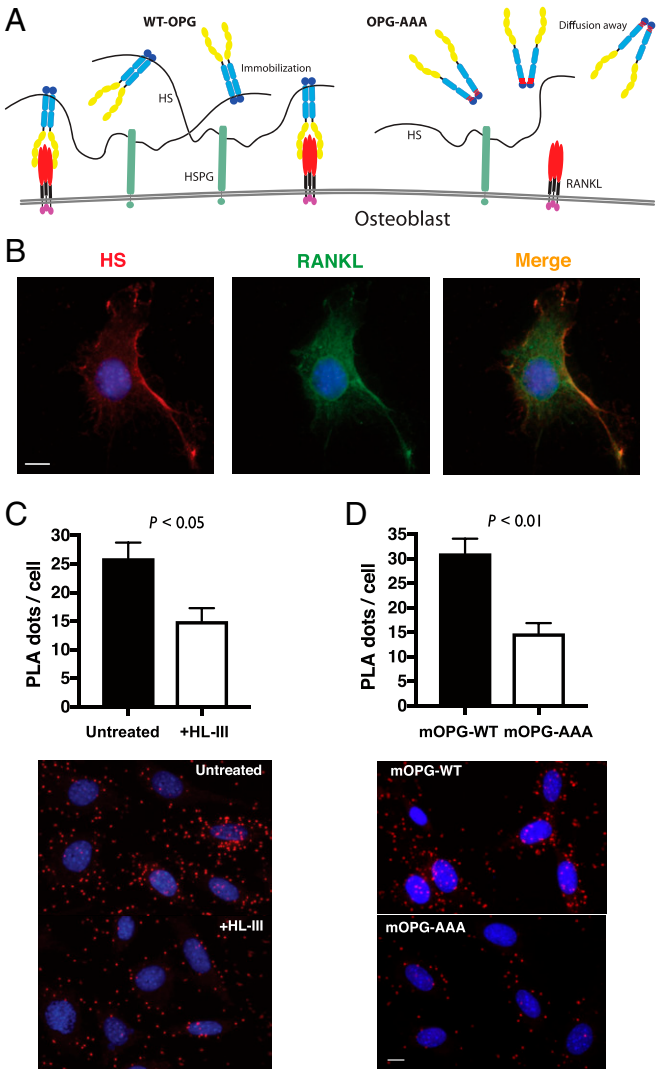

Fig. 4. HS promotes OPG–RANKL interaction at osteoblast surface. (*A*) Proposed model for the role of HS in OPG–RANKL interactions. When secreted OPG is immobilized by HSPG, HSPG facilitates the interaction between bound OPG and membrane-attached RANKL, which is located near HSPG. OPG-AAA diffuses away from cell membrane due to its deficiency in HS binding, which makes binding to membrane-attached RANKL much more difficult. (*B*) Colocalization of HS and RANKL on osteoblast surface. MC3T3^{RANKL} cells were costained with an anti-HS mAb (10E4) and a polyclonal anti-RANKL antibody. (*C*) OPG–RANKL complex formation on osteoblast surface with or without HL-III treatment. All samples were incubated with 10 ng/mL mOPG-WT prior to fixation. (*D*) OPG–RANKL complex formation when cells were preincubated with either mOPG-WT or mOPG-AAA, both at 10 ng/mL. For *C* and *D*, each red dot indicates an interaction between OPG and RANKL. Nuclei are shown in blue. $n = 4$ to 6. Error bars represent SD. *P* value was determined by two-way Student's *t* test. Data are representative of three separate assays. (Scale bars, 10 μm.)

reduction of bone volume (3, 4). Our finding strongly suggests that in vivo, the interaction between OPG and HS is essential for the normal function of OPG, without which the OPG is nearly nonfunctional.

A recent study has found that *Oc-Cre;Ext1$^{f/f}$* mice also display osteoporotic phenotype (18). Ext1 is an enzyme that is essential for HS polymerization, without which the HS biosynthesis will be completely halted (8). As a result, the osteoblast lineage cells in *Oc-Cre;Ext1$^{f/f}$* mice express no HS on their cells surface. In contrast, Hs2st is an enzyme that adds sulfate to the 2-*O*-position of the already polymerized HS chain. In the absence of Hs2st only, the fine structure of HS is altered, while the overall sulfation level and the quantity of HS expressed by Hs2st-deficient cells are generally comparable with WT cells (*SI Appendix*, Fig. S5) (21, 23). Therefore, it is expected that our *Oc-Cre;Hs2st$^{f/f}$* mice had a much smaller alteration on the HS landscape on osteoblast surface compared with the *Oc-Cre;Ext1$^{f/f}$* mice. In addition, since only a small fraction of HS-binding proteins has been shown to rely strictly on 2-*O*-sulfation (bFGF and OPG being two examples) (10), deletion of Hs2st in osteoblast is expected to have a limited impact on many other HS-binding proteins that normally interact with osteoblast HS. Despite this, we still cannot exclude the possibility that the functions of some HS-binding proteins are altered in *Oc-Cre;Hs2st$^{f/f}$* mice. However, in light of the highly similar phenotypes between *opg$^{AAA/AAA}$* and *Oc-Cre;Hs2st$^{f/f}$* mice, it is unlikely that another HS-binding protein makes significant contribution to the osteoporotic phenotype.

In contrast to the deletion of Hs2st, the total loss of HS imposed by deletion of Ext1 would abolish binding of all HS-binding proteins, which would make interpretation of phenotype much more complicated. Indeed, the bone phenotypes of *Oc-Cre;Ext1$^{f/f}$* and *Oc-Cre;Hs2st$^{f/f}$* mice are distinct in several regards. For example, the long bones of Oc-Cre;*Ext1$^{f/f}$* mice display clear morphological defects such as thickening of metaphysis and collapse of secondary ossification center (18), while the morphology of the *Oc-Cre;Hs2st$^{f/f}$* mice is normal. In addition, the long bones of our *opg$^{AAA/AAA}$* mice also did not display any morphological defects, and such defects were not reported in *opg*-null mice either (3, 4). This evidence suggests that impaired OPG–HS interaction is not the only factor that contributes to the bone phenotype exhibited by *Oc-Cre;Ext1$^{f/f}$* mice. It is highly likely that other yet unidentified HS-binding proteins also contribute to the bone phenotype observed in *Oc-Cre;Ext1$^{f/f}$* mice.

Mechanistically, we propose that cell surface HSPGs immobilize OPG on the membrane, which greatly promotes its inhibition of membrane-attached RANKL (Fig. 4*A*). Indeed, we have presented evidence by coimmunofluorescence and PLA assay that these interactions truly occur at the cell surface (Fig. 4). When HS is absent from the osteoblast cell surface, or when OPG is incapable of binding HS (in the case of OPG-AAA mutant), OPG has a lower chance of binding RANKL at the osteoblast cell surface. In addition to immobilizing and concentrating OPG at the cell surface, it is possible that HS also promotes OPG–RANKL interaction in other ways. For example, we have shown that HS binding induces a substantial conformational change of OPG dimer (7), which might facilitate more efficient OPG–RANKL interactions. In addition, as HSPG is known to be involved in receptor internalization, and HSPG, OPG, and RANKL do form a stable ternary complex (7), it is also possible that HSPG is involved in RANKL internalization. RANKL internalization would further reduce the bioavailability of RANKL at cell surface and help dampen osteoclastogenesis.

In summary, our study has provided strong genetic evidence that OPG functions in an HS-dependent manner and established HSPG as an integral component of the OPG/RANKL/RANK pathway. As OPG also plays other biological functions such as inhibiting vascular calcification and promoting pulmonary vascular remodeling, skeletal muscle strength, and liver steatosis (24–28), it would be interesting to examine whether HS also regulates OPG functions in these systems. The *opg^{AAA}* mice reported here would certainly be an invaluable tool to better understand the diverse physiological functions of OPG.

Materials and Methods

Generation of *opg^{AAA}* Knock-In Mice. The knock-in project was performed by Applied StemCell, Inc. Briefly, the synthesized sgRNA (which targets exon 5 of mouse *opg* gene as shown in Fig. 1*D*), repair template ssODN, and messenger RNA encodes for CRISPR-associated protein 9 (Cas9) were microinjected into

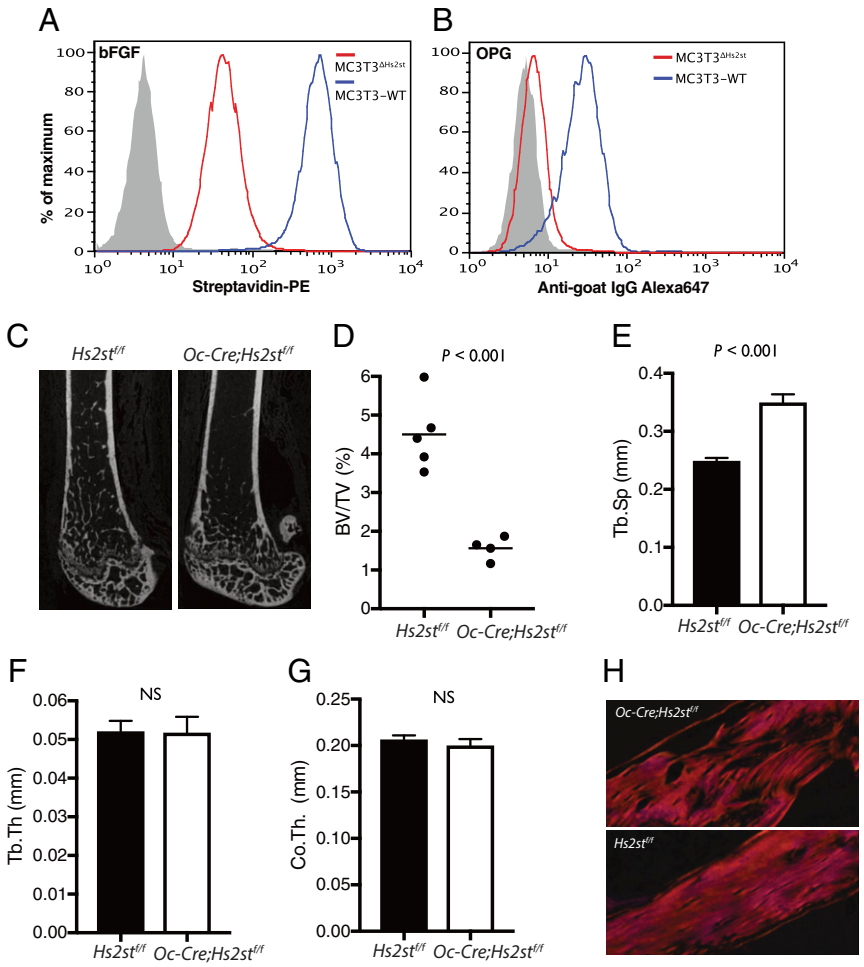

Fig. 5. *Oc-Cre;Hs2st*$^{f/f}$ mice develop osteoporosis due to the essential role of 2-*O*-sulfation in HS–OPG interaction. (*A*) Binding of biotin-bFGF (basic fibroblast growth factor) to MC3T3-WT and MC3T3$^{\Delta Hs2st}$ is determined by FACS. PE, phycoerythrin. IgG, immunoglobulin G. (*B*) Binding of mOPG to MC3T3-WT and MC3T3$^{\Delta Hs2st}$ is determined by FACS. (*C*) Representative μCT images of the femurs. (*D*) Trabecular BV/TV of femurs. (*E*) Trabecular separation (Tb.Sp), (*F*) trabecular thickness (Tb.Th), and (*G*) cortical thickness (Co.Th.) of femurs. All values are from 10-wk-old male mice. $n = 4$ to 5. Error bars represent SD. *P* value was determined by two-way Student's *t* test. NS, not significant. (*H*) Polarized light microscopy of cortical bone shows woven pattern in *Oc-Cre;Hs2st*$^{f/f}$ mice and lamellar pattern of *Hs2st*$^{f/f}$ mice.

one cell-stage fertilized egg of C57BL6J strain, which was then surgically transferred into pseudopregnant foster mothers also of C57BL6J background. Through CRIPSR-based homology-directed repair, the triple mutations were introduced into the *opg* locus. The pups were screened by next generation sequencing, and the mice that bore correct mutations were mated to WT C57BL6 mice to confirm germline transmission of the mutations. The F1 heterozygous mice were bred together to generate homozygous offspring. All animal works in this study have been approved by the institutional animal care and use committee of the University at Buffalo.

Generation of Oc-Cre;*Hs2st*$^{f/f}$ Mice. Conditional *Hs2st* knockout mice were generated by crossing the *Hs2st*$^{f/f}$ mice (gift from Jeffery Esko, University of California San Diego, La Jolla, CA) and Oc-Cre transgenic mice (Jackson Laboratory). All experiments were performed with mice with a complete C57BL/6J background. Genotyping of the mice was performed by PCR as previously described (23).

Radiographic Examination (X-Ray) and μCT Analysis. X-ray was performed on a Faxitron X-Ray specimen radiography system using an energy of 35 kV and an exposure time of 60 s. Mouse femurs from different ages of WT, *opg*^{AAA}, *Oc-Cre;Hs2st*$^{f/f}$, and *Hs2st*$^{f/f}$ mice were harvested and fixed for 48 h in 10% neutral buffered formalin. A quantitative analysis of the gross bone morphology and microarchitecture was performed using the Skyscan 1172 microCT system (New York University, School of Dentistry, μCT Core). Three-dimensional reconstruction and bone microarchitecture analysis were performed using AnalyzePro (AnalyzeDirect Inc).

Immunostaining. RANKL stably expressing MC3T3 cell (MC3T3^{RANKL}) was made by transfecting MC3T3-E1 cells with pUNO1-RANKL vector using Jetprime kit (polyplus transfection). The transfected cells were seeded into a 96-well plate at 0.5 cells per well. Cells were cultured with Blasticidin (5 μg/mL) until single-cell clones grew to colonies. RANKL expression was analyzed by staining with a rat anti-mouse RANKL mAb (IK22/5; Thermo Fisher). A clone with medium expression level of RANKL was selected for the immunostaining and PLA.

MC3T3^{RANKL} cells were cultured on cell culture chambered coverslips (culturewell; Invitrogen) and fixed with 4% paraformaldehyde (PFA). Immunofluorescence staining was performed using 0.1 μg/mL murine anti-HS mAb 10E4 (US Biological) and 1 μg/mL goat polyclonal anti-RANKL (R&D Systems), followed by donkey anti-mouse IgG NL-557 (R&D Systems) and donkey anti-goat IgG Alexa488 (Thermo Fisher). Images were taken with a Nikon Ci-S fluorescence microscope and merged using ImageJ software.

Proximity Ligation Assay. MC3T3^{RANKL} cells were cultured on cell culture chambered coverslips. Selected wells were treated with HL-III to remove cell surface HS (5 mU/mL, 15 min, room temperature). Cells were then incubated with 10 ng/mL recombinant WT mOPG (or OPG-AAA mutant in selected wells) at 4 °C for 1 h before fixation with 4% PFA. The PLA (Duolink in situ; Sigma-Aldrich) was performed according to the manufacturer's protocol using a rabbit polyclonal antibody to mOPG (made in house) and a goat monoclonal antibody to RANKL (R&D Systems) at 50 ng/mL as primary antibody. After incubating with oligonucleotide-conjugated secondary antibodies (to rabbit and goat IgG, respectively), the hybridized oligonucleotides were enzymatically amplified by rolling circle amplification. The amplified DNA was

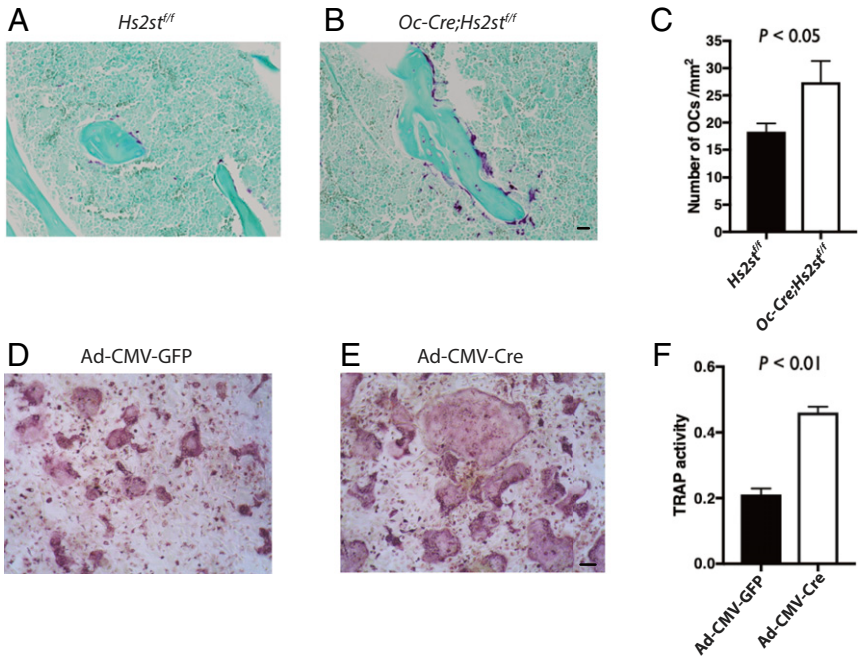

Fig. 6. Osteoclastogenesis is enhanced in Oc-Cre;*Hs2st*$^{f/f}$ mice. (*A* and *B*) TRAP staining of paraffin sections of *Hs2st*$^{f/f}$ and Oc-Cre;*Hs2st*$^{f/f}$ tibias. (*C*) Quantification of osteoclasts (OCs) in tibia sections. $n = 6$. (*D* and *E*) Osteoblasts isolated from *Hs2st*$^{f/f}$ were infected with adenovirus constructs Ad-CMV-GFP and AD-CMV-Cre to generate control and Hs2st-deficient osteoblasts, respectively. These cells were cocultured with WT BMM. Mature osteoclasts are visualized by TRAP staining. (*F*) The extent of osteoclastogenesis in coculture was assessed by an enzymatic assay of TRAP activity in whole-cell lysate. $n = 3$. Error bars represent SD. *P* value was determined by two-way Student's *t* test. Data are representative of at least three separate assays. (Scale bars, 50 μm.)

visualized by addition of complementary Texas Red-labeled oligonucleotides. Each complex appeared as intense red dots. For negative control, 50 ng/mL anti-mOPG and normal goat IgG were used as primary antibodies. Less than three PLA dots per cell were observed in these control wells.

Generation of 2-*O*-Sulfation Deficiency MC3T3 Cells (MC3T3$^{\Delta Hs2st}$). A small guide RNA was designed to target the first exon of murine Hs2st (5′-CACCGG CGGTGGTGGCCTTCGCGG-3′). The guide RNA was cloned into pSpCas9-puro vector (Addgene) and transfected into MC3T3-E1 cells. The transfected cells were selected with puromycin (1.5 μg/mL). After 10 d, the surviving cells were seeded into a 96-well plate at 0.5 cells per well to obtain single-cell clone. The expanded single-cell clone was analyzed by bFGF binding assay to verify inactivation of Hs2st and the homogeneity of the clone. Immunostaining of cell surface HS was performed using 0.1 μg/mL 10E4 as described above in *Immunostaining*.

Fluorescence-Activated Cell Sorting. MC3T3-E1 cells and MC3T3$^{\Delta Hs2st}$ were lifted from culture dish using Accutase (Biolegend) and incubated with biotin-bFGF (10 ng/mL) or mOPG (10 ng/mL) in 100 μL phosphate buffered saline and 0.1% bovine serum albumin for 1 h at 4 °C. Bound mOPG was stained with goat anti-mouse OPG (400 ng/mL, AF459; R&D Systems) for 1 h at 4 °C, followed by anti-goat IgG-Alexa 647 (1:1,000; ThermoFisher Scientific) for 30 min and analyzed by flow cytometry. Biotin-bFGF was stained by streptavidin-PE for 15 min and analyzed by flow cytometry.

Coculture Osteoclastogenesis Assay. Primary osteoblasts were isolated from calvaria of 5- to 8-d-old WT or *opg*^{AAA} mice following an established protocol (29). WT and *opg*^{AAA} osteoblasts (3.5×10^3 cells per well) were seeded in a 96-well plate the day before starting the coculture. Freshly isolated bone marrow cells from one leg of WT mice were suspended in 10 mL α-MEM containing 10% fetal bovine serum, 1× penicillin/streptomycin, 10^{-7} M dexamethasone, and 10^{-8} M 1α- and 25-dihydroxyvitamin D3; 100 μL bone marrow cells were added into each well. The medium was replaced every 2 d thereafter until the appearance of giant osteoclasts. To visualize osteoclasts, the cells were fixed and stained for TRAP activity using an Leukocyte Acid Phosphatase kit (Sigma). For quantitative measurement of TRAP activity, cells were lysed with 50 μL lysis buffer (50 mM tris(hydroxymethyl)aminomethane, pH 7.5, 150 mM NaCl, 1% Nonidet P-40) for 30 min at 4 °C; 10 μL lysate was then mixed with 50 μL TRAP assay buffer containing 0.5 M sodium acetate, 10 mM tartrate, and 10 mM *p*-nitrophenyl phosphate substrate and incubated at 37 °C for 15 min. The reaction was stopped by adding 50 μL 0.5 N NaOH, and the absorbance at 405 nm was measured by a plate reader.

Statistical Analysis. All data are expressed as means ± SD. Statistical significance of differences between experimental and control groups was analyzed by two-tailed unpaired Student's *t* test using GraphPad Prism software (GraphPad Software Inc.). *P* value < 0.05 was considered significant.

All data necessary for replication are included in *Materials and Methods* and in *SI Appendix, Materials and Methods*. The *opg*^{AAA} knock-in mice as well as MC3T3^{RANKL} cells and MC3T3$^{\Delta Hs2st}$ cells will be available on request by qualified researchers for their own use.

ACKNOWLEDGMENTS. We thank Dr. Jeffery Esko (University of California San Diego) for providing *Hs2st*$^{f/f}$ mice and the μCT Core of School of Dentistry, New York University (supported by NIH Grant S10 OD010751) for providing μCT scan. The work is supported by NIH Grants AR070179 (to D.X.) and HL094463 (to D.X.). The content is solely the responsibility of the authors and does not necessarily represent the official views of the NIH.

1. W. S. Simonet *et al*., Osteoprotegerin: A novel secreted protein involved in the regulation of bone density. *Cell* **89**, 309–319 (1997).
2. D. L. Lacey *et al*., Osteoprotegerin ligand is a cytokine that regulates osteoclast differentiation and activation. *Cell* **93**, 165–176 (1998).
3. N. Bucay *et al*., osteoprotegerin-deficient mice develop early onset osteoporosis and arterial calcification. *Genes Dev.* **12**, 1260–1268 (1998).
4. A. Mizuno *et al*., Severe osteoporosis in mice lacking osteoclastogenesis inhibitory factor/osteoprotegerin. *Biochem. Biophys. Res. Commun.* **247**, 610–615 (1998).
5. H. Yasuda *et al*., Osteoclast differentiation factor is a ligand for osteoprotegerin/osteoclastogenesis-inhibitory factor and is identical to TRANCE/RANKL. *Proc. Natl. Acad. Sci. U.S.A.* **95**, 3597–3602 (1998).
6. J. Xiong *et al*., Soluble RANKL contributes to osteoclast formation in adult mice but not ovariectomy-induced bone loss. *Nat. Commun.* **9**, 2909 (2018).
7. M. Li, S. Yang, D. Xu, Heparan sulfate regulates the structure and function of osteoprotegerin in osteoclastogenesis. *J. Biol. Chem.* **291**, 24160–24171 (2016).
8. J. D. Esko, S. B. Selleck, Order out of chaos: Assembly of ligand binding sites in heparan sulfate. *Annu. Rev. Biochem.* **71**, 435–471 (2002).

9. J. R. Bishop, M. Schuksz, J. D. Esko, Heparan sulphate proteoglycans fine-tune mammalian physiology. *Nature* **446**, 1030–1037 (2007).
10. D. Xu, J. D. Esko, Demystifying heparan sulfate-protein interactions. *Annu. Rev. Biochem.* **83**, 129–157 (2014).
11. J. P. Li *et al*., Targeted disruption of a murine glucuronyl C5-epimerase gene results in heparan sulfate lacking L-iduronic acid and in neonatal lethality. *J. Biol. Chem.* **278**, 28363–28366 (2003).
12. H. Habuchi *et al*., Mice deficient in heparan sulfate 6-O-sulfotransferase-1 exhibit defective heparan sulfate biosynthesis, abnormal placentation, and late embryonic lethality. *J. Biol. Chem.* **282**, 15578–15588 (2007).
13. K. Grobe *et al*., Cerebral hypoplasia and craniofacial defects in mice lacking heparan sulfate Ndst1 gene function. *Development* **132**, 3777–3786 (2005).
14. S. L. Bullock, J. M. Fletcher, R. S. Beddington, V. A. Wilson, Renal agenesis in mice homozygous for a gene trap mutation in the gene encoding heparan sulfate 2-sulfotransferase. *Genes Dev.* **12**, 1894–1906 (1998).
15. C. A. Nelson, J. T. Warren, M. W. Wang, S. L. Teitelbaum, D. H. Fremont, RANKL employs distinct binding modes to engage RANK and the osteoprotegerin decoy receptor. *Structure* **20**, 1971–1982 (2012).
16. X. Luan *et al*., Crystal structure of human RANKL complexed with its decoy receptor osteoprotegerin. *J. Immunol.* **189**, 245–252 (2012).
17. Y. Xiao *et al*., Dimerization interface of osteoprotegerin revealed by hydrogen-deuterium exchange mass spectrometry. *J. Biol. Chem.* **293**, 17523–17535 (2018).
18. S. Nozawa *et al*., Osteoblastic heparan sulfate regulates osteoprotegerin function and bone mass. *JCI Insight* **3**, e89624 (2018).
19. X. Bai, J. D. Esko, An animal cell mutant defective in heparan sulfate hexuronic acid 2-O-sulfation. *J. Biol. Chem.* **271**, 17711–17717 (1996).
20. J. van den Born *et al*., Novel heparan sulfate structures revealed by monoclonal antibodies. *J. Biol. Chem.* **280**, 20516–20523 (2005).
21. J. Axelsson *et al*., Inactivation of heparan sulfate 2-O-sulfotransferase accentuates neutrophil infiltration during acute inflammation in mice. *Blood* **120**, 1742–1751 (2012).
22. K. Yamaguchi *et al*., Characterization of structural domains of human osteoclastogenesis inhibitory factor. *J. Biol. Chem.* **273**, 5117–5123 (1998).
23. K. I. Stanford *et al*., Heparan sulfate 2-O-sulfotransferase is required for triglyceride-rich lipoprotein clearance. *J. Biol. Chem.* **285**, 286–294 (2010).
24. C. Zhang *et al*., Osteoprotegerin promotes liver steatosis by targeting the ERK-PPAR-γ-CD36 pathway. *Diabetes* **68**, 1902–1914 (2019).
25. H. Min *et al*., Osteoprotegerin reverses osteoporosis by inhibiting endosteal osteoclasts and prevents vascular calcification by blocking a process resembling osteoclastogenesis. *J. Exp. Med.* **192**, 463–474 (2000).
26. S. S. Dufresne *et al*., Osteoprotegerin protects against muscular dystrophy. *Am. J. Pathol.* **185**, 920–926 (2015).
27. N. Bonnet, L. Bourgoin, E. Biver, E. Douni, S. Ferrari, RANKL inhibition improves muscle strength and insulin sensitivity and restores bone mass. *J. Clin. Invest.* **129**, 3214–3223 (2019).
28. N. D. Arnold *et al*., A therapeutic antibody targeting osteoprotegerin attenuates severe experimental pulmonary arterial hypertension. *Nat. Commun.* **10**, 5183 (2019).
29. A. D. Bakker, J. Klein-Nulend, Osteoblast isolation from murine calvaria and long bones. *Methods Mol. Biol.* **816**, 19–29 (2012).